Electronic Supplementary Material (ESI) for Materials Horizons.
This journal is © The Royal Society of Chemistry 2024

Supporting Information

Trace SO_2 Capture within the Engineered Pore Space using a Highly Stable SnF_6^{2-}-pillared MOF

Weiwei Li,[†] Can Cheng,[†] Guanqun Gao,[†] Haomiao Xu,[†] Wenjun Huang,[†] Zan Qu,[†,*] and Naiqiang Yan[†]

[†] School of Environmental Science and Engineering, Shanghai Jiao Tong University, 800 Dongchuan Road, Shanghai 200240, China

quzan@sjtu.edu.cn

Section S1. Chemicals and materials
Section S2. Methodology
Section S3. Single-crystal X-ray diffraction
Section S4. Density functional theory (DFT) calculations
Section S5. Grand Canonical Monte Carlo (GCMC) simulations
Section S6. Figures and Tables
Scheme S1. A schematic illustration of breakthrough experiments in the fixed-bed reaction system.
Scheme S2. A schematic illustration of adsorption-desorption cycling tests in the in-situ thermal-gravimetric balance system.
Figure S1. (A) Photography of synthesis of single-crystal SNFSIX-Cu-TPA utilizing NMR glass tubes with an outer diameter of 5 mm via the interfacial diffusion method. (B) Photography of synthesis of powder SNFSIX-Cu-TPA utilizing 20-mL glass tubes with an outer diameter of 20 mm via the interfacial diffusion method.
Figure S2. Photography of single-crystal SNFSIX-Cu-TPA.
Figure S3. Schematic views of the 3D frameworks and calculated pore surface of SNFSIX-Cu-TPA. Accessible Connolly surface determined by using a probe with a radius of 1.2 Å. The voids of SNFSIX-Cu-TPA generated with a probe with a radius of 1.2 Å.
Figure S4. PXRD pattern of as-synthesized and simulated SIFSIX-Cu-TPA.
Figure S5. Calculation of BET surface area for SNFSIX-Cu-TPA and SIFSIX-Cu-TPA derived from nitrogen adsorption isotherm at 77 K.
Figure S6. Experimental SO_2 adsorption isotherms at 298/273 K and DSLF model fitting curve of SNFSIX-Cu-TPA.
Figure S7. Experimental CO_2 adsorption isotherms at 298/273 K and DSLF model fitting curve of SNFSIX-Cu-TPA.
Figure S8. Experimental N_2 adsorption isotherms at 298/273 K and DSLF model fitting curve of SNFSIX-Cu-TPA.
Figure S9. Experimental SO_2 adsorption isotherms at 298/273 K and DSLF model fitting curve of SIFSIX-Cu-TPA.
Figure S10. Experimental CO_2 adsorption isotherms at 298/273 K and DSLF model fitting curve of SIFSIX-Cu-TPA.
Figure S11. Experimental N_2 adsorption isotherms at 298 K and DSLF model fitting curve of SNFSIX-Cu-TPA.
Figure S12. (A) The SO_2/CO_2 and SO_2/N_2 sorption selectivity of SIFSIX-Cu-TPA based on IAST for the 10/90, 1/99 and 50/50 mixture of SO_2/CO_2 or SO_2/N_2 at 298 K.
Figure S13. Heat of adsorption (Q_{st}) for both SO_2 and CO_2 as a function of the gas loading amount determined from a viral fit to isotherms collected at 298 K and 273 K.
Figure S14. Snapping shots of within the SNFSIX-Cu-TPA structure at 1 bar and 298 K from GCMC simulation results.
Figure S15. The optimized structure of SNFSIX-Cu-TPA for DFT calculation.
Figure S16. The optimized structure of SIFSIX-Cu-TPA for DFT calculation.
Figure S17. The DFT optimized gas adsorption configuration in SIFSIX-Cu-TPA at Binding sites 1 of SO_2 and CO_2.
Figure S18. Experimental fix-bed breakthrough curves of three cycling tests in the $SO_2/CO_2/N_2$ mixture on SNFSIX-Cu-TPA at 298 K by activation at room temperature under vacuum for 12 h. (2000 ppm SO_2, 10 vol.% CO_2, 89.8 vol.% N_2; flow rate: 20 mL/min).

Figure S19. Repeated adsorption-desorption isotherms of SO_2 at 298 K and 1 bar on SNFSIX-Cu-TPA.
Table S1. Single crystal data and structure refinement for SNFSIX-Cu-TPA.
Table S2. The adsorption capacities of SO_2 on various MOFs at 298 K.
Table S3. BET report for MFSIX-Cu-TPA.
Table S4. Comparison of utilization efficiency per anions in anion pillared MOFs used in SO_2 and CO_2 adsorption.
Table S5. Fitting parameters of DSLF model in SNFSIX-Cu-TPA for adsorption isotherms at 298/273 K.
Table S6. Fitting parameters of DSLF model in SIFSIX-Cu-TPA for adsorption isotherms at 298/273 K.
Table S7. Virial fittings for calculating isosteric heat of adsorption of SO_2 and CO_2 on two MFSIX-Cu-TPA.
Table S8. Calculated the static binding energies in MFSIX-Cu-TPA

Number of pages:25

Number of figures: 19

Number of tables: 8

Section S1. Chemicals and materials

All chemicals are commercially available and used directly without further purification.

Name	Supplier	Purity (%)	CAS-Number
$Cu(NO_3)_2 \cdot 3H_2O$	Macklin	99	100-21-0
Tri(pyridin-4-yl) amine (TPA)	Bide	98	153467-50-6
$(NH_4)_2SnF_4$	Macklin	99	16919-24-7
$(NH_4)_2SiF_4$	Aladdin	99	16919-19-0
Methanol	Macklin	99.5	64-17-5
2 vol% SO_2 in N_2	Wetry (Shanghai)	99.999	7727-37-9
CO_2	Wetry (Shanghai)	99.999	7727-37-9
N_2	Air liquid	99.5	7727-37-9
deionized water H_2O	Laboratory	Self-made	-

88

89

Section S2. Equipment setup

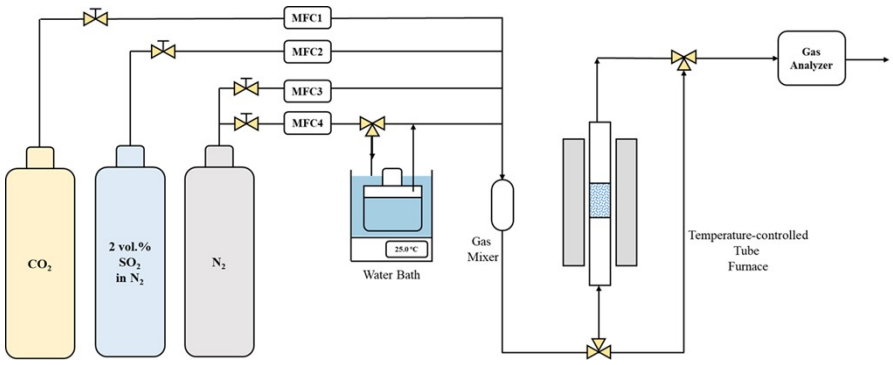

Scheme S1. A schematic illustration of breakthrough experiments in the fixed-bed reaction system.

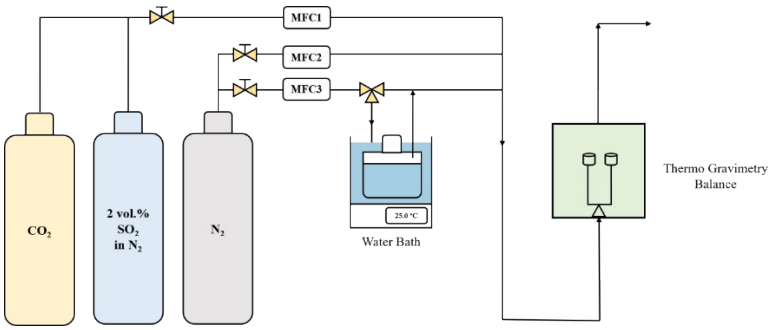

Scheme S2. A schematic illustration of adsorption-desorption cycling tests in the *in-situ* thermal-gravimetric balance system.

Section S3. Single-crystal X-ray diffraction:

Single-crystal X-ray diffraction: Single-crystal X-ray diffraction data were acquired by a Bruker D8 Venture Metaljet PHOTON II diffractometer equipped with GaKα radiation (λ = 1.34139 Å). The suitable crystal was selected and kept at 193 K during data collection. The structural determination was performed using Olex2, employing the Direct Methods with the SHELXS, followed by refinement using the SHELXL refinement package and Least Squares minimization. Anisotropic refinement was applied to all nonhydrogen atoms, while hydrogen atoms bonded with carbon atoms were included at calculated positions and refined using a riding model.

Section S4. Density functional theory (DFT) calculations

The first-principles density functional theory (DFT) calculations for the determination of static adsorption energies were carried out using the CP2K code. The adsorption energy can provide valuable insights into the interactions between the SO_2/CO_2/N_2 and the MFSIX-Cu-TPA. All the simulations employed a combination of Gaussian and plane-wave basis sets. The core electrons were represented with norm-conserving Goedecker-Teter-Hutter pseudopotentials. Additionally, the valence electron wave function was expanded in a double-zeta basis set with polarization functions. This is added by an auxiliary plane wave basis set. A kinetic cut-off energy of 360 eV was utilized to ensure accurate calculations. The exchange-correlation function employed in these calculations was the Perdew-Burke-Enzerhof (PBE) generalized gradient approximation. Each configuration was optimized with the Broyden-Fletcher-Goldfarb-Shanno (BGFS) algorithm, with self-consistent field (SCF) convergence criteria of 1.0×10^{-6} au. Grimme's DFT-D3 model was also utilized to account for van der Waals interactions, providing a more accurate description of the whole system.

Section S5. Grand Canonical Monte Carlo (GCMC) simulations

Grand Canonical Monte Carlo (GCMC) simulations of single-component adsorption isotherms were all performed using RASPA package.[1]The structure of SNFSIX-Cu-TPA was firstly optimized via DFT geometry optimization in the Section S5. All Monte Carlo simulations were performed using the Lennard-Jones (L-J) potential in a rigid framework. The Lennard-Jones parameters for adsorbate-host interactions were obtained using the Lorentz-Berthelot mixing rules. The force field parameters for CO_2 and N_2 were taken from the TraPPE force field, where both molecules were considered rigid.[2] Additionally, the force field parameters for SO_2 were taken from Ketko's optimized SO_2 model, which includes a harmonic O–S–O bending angle potential with the S–O bond length fixed.[3] Van der Waals interactions were calculated using a 12 Å cutoff, and the minimum image convention was satisfied using a 2x2x2 supercell. Besides, the Ewald summation method was used to compute Coulomb interactions. For all GCMC simulations, sampling began after $1x10^4$ initialization cycles and thermodynamic properties were sampled over the next 10^5 cycles.

Section S6. Figures and Tables

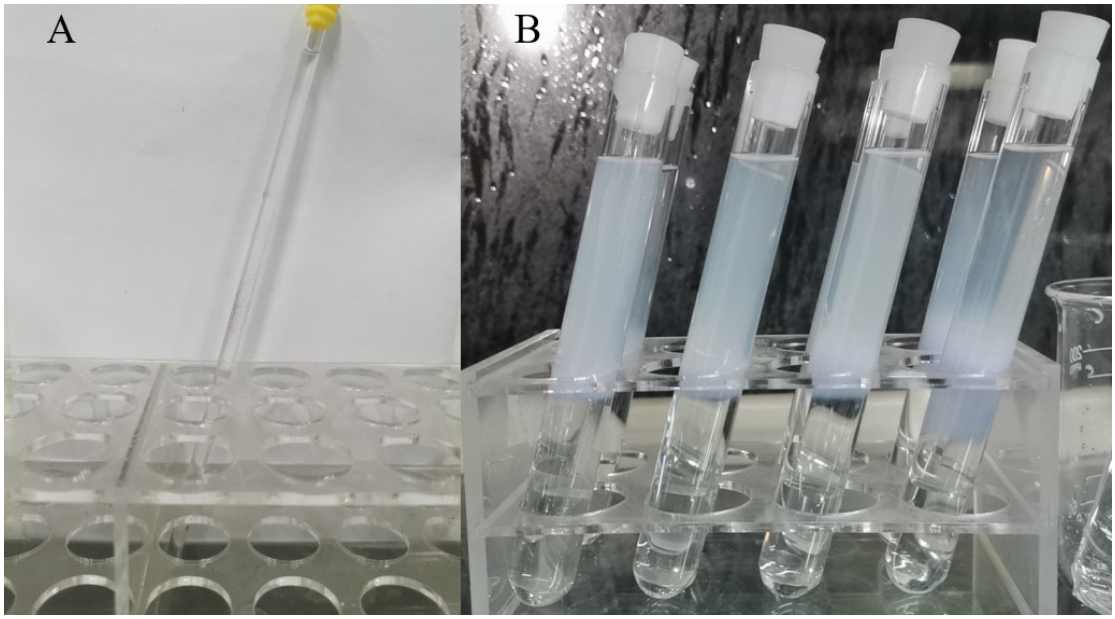

Figure S1. (A) Photography of synthesis of single-crystal SNFSIX-Cu-TPA utilizing NMR glass tubes with an outer diameter of 5 mm via the slow diffusion method. (B) Photography of synthesis of powder SNFSIX-Cu-TPA utilizing 20-mL glass tubes with an outer diameter of 20 mm via the interfacial diffusion method.

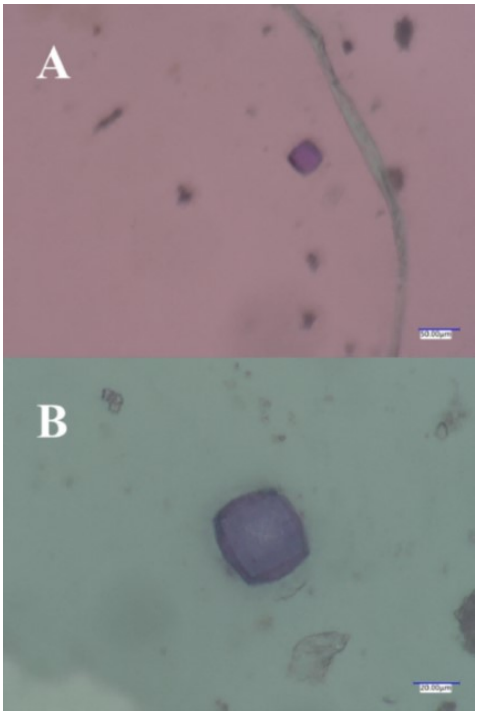

Figure S2. Photography of single-crystal SNFSIX-Cu-TPA.

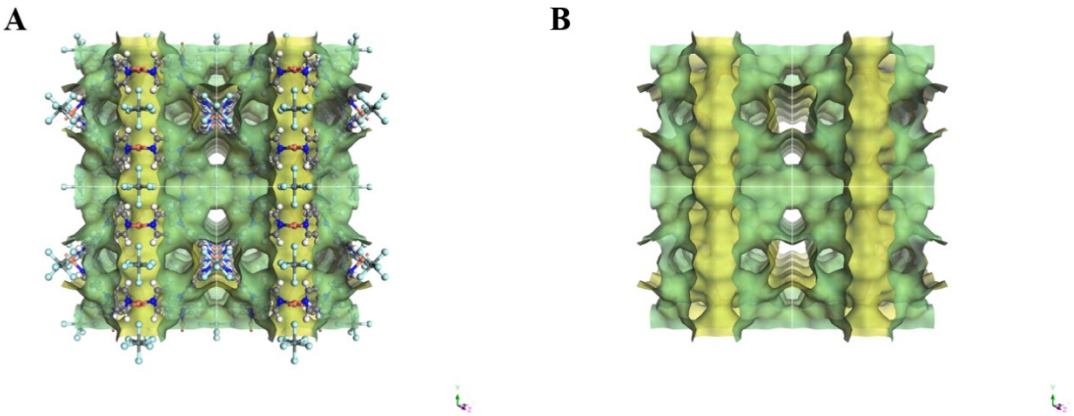

147

148 **Figure S3.** Schematic views of the 3D frameworks and calculated pore surface of SNFSIX-Cu-

149 TPA. Accessible Connolly surface determined by using a probe with a radius of 1.2 Å. The voids

150 of SNFSIX-Cu-TPA generated with a probe with a radius of 1.2 Å.

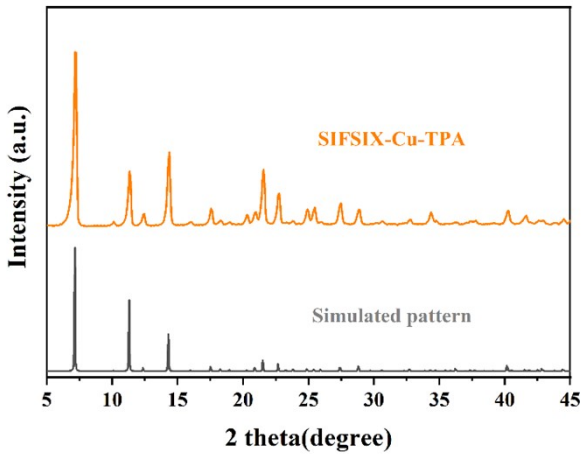

151

152 **Figure S4.** PXRD pattern of as-synthesized and simulated SIFSIX-Cu-TPA.

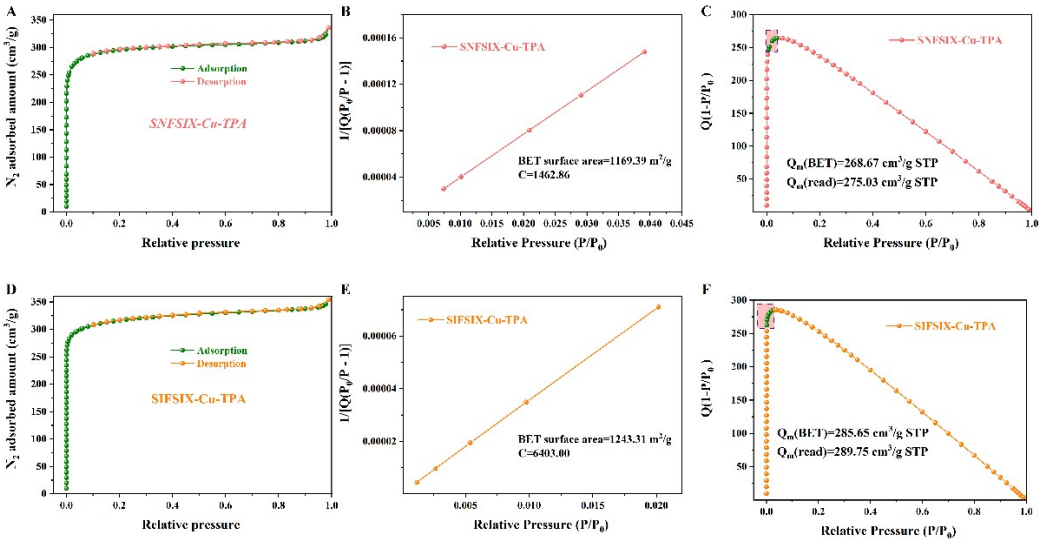

153

154 **Figure S5.** Calculation of BET surface area for SNFSIX-Cu-TPA and SIFSIX-Cu-TPA derived

155 from nitrogen adsorption isotherm at 77 K.

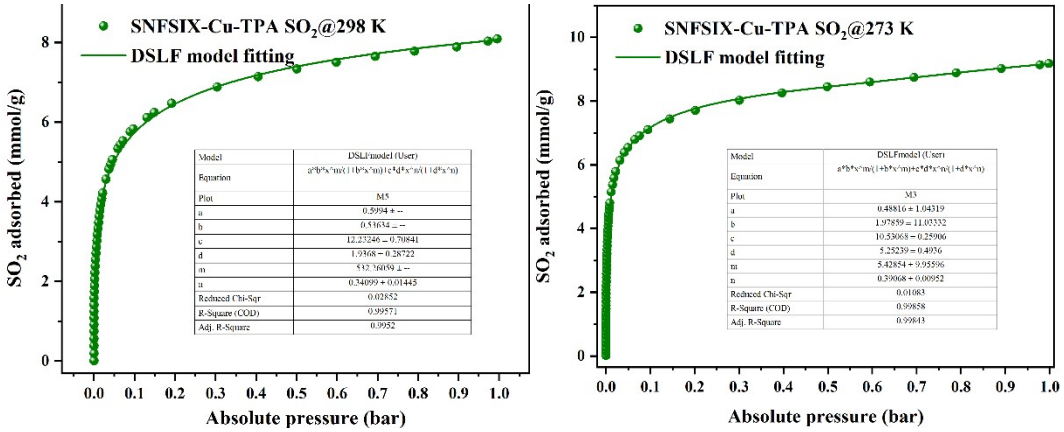

156

157 **Figure S6.** Experimental SO_2 adsorption isotherms at 298/273 K and DSLF model fitting curve of

158 SNFSIX-Cu-TPA.

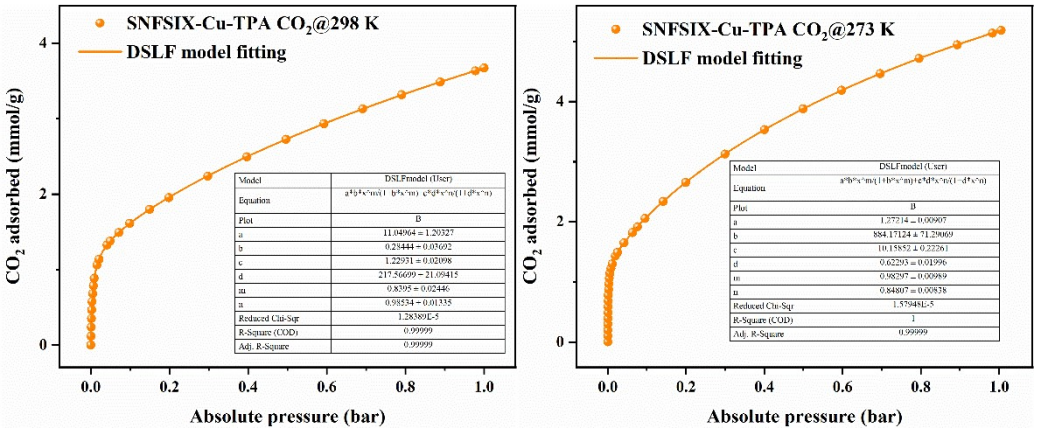

159

160 **Figure S7.** Experimental CO_2 adsorption isotherms at 298/273 K and DSLF model fitting curve of

161 SNFSIX-Cu-TPA.

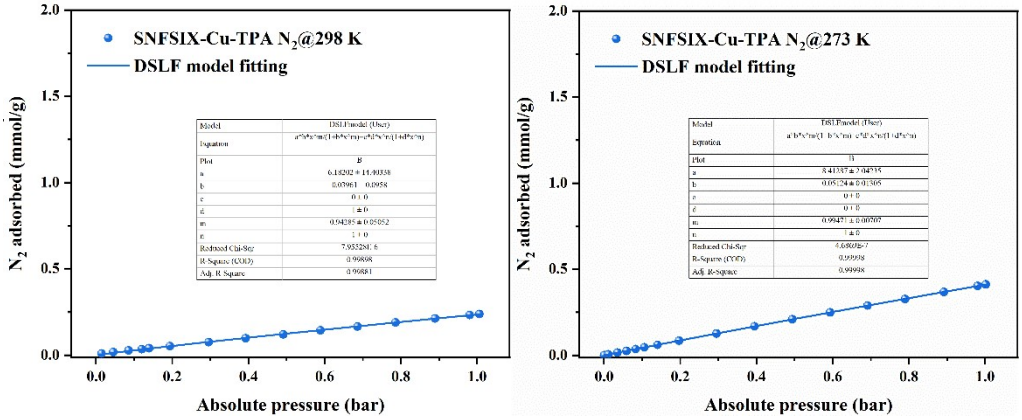

162

163 **Figure S8.** Experimental N_2 adsorption isotherms at 298/273 K and DSLF model fitting curve of

164 SNFSIX-Cu-TPA.

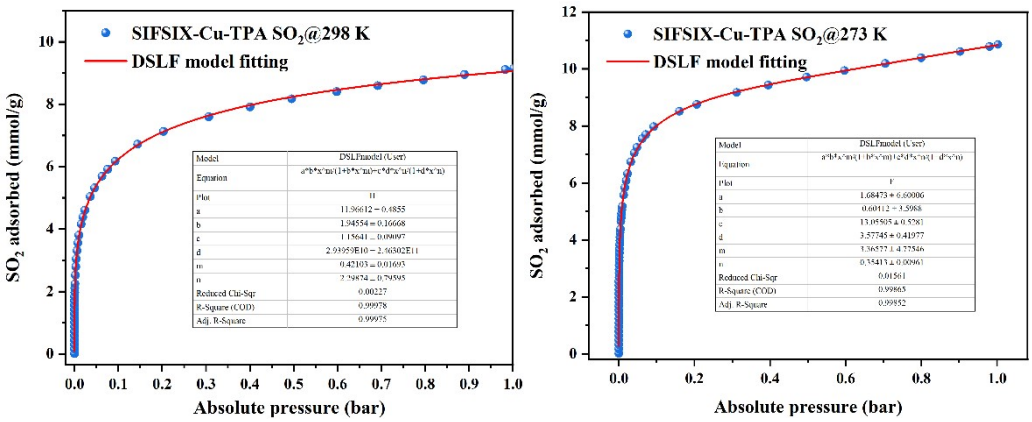

Figure S9. Experimental SO_2 adsorption isotherms at 298/273 K and DSLF model fitting curve of SIFSIX-Cu-TPA.

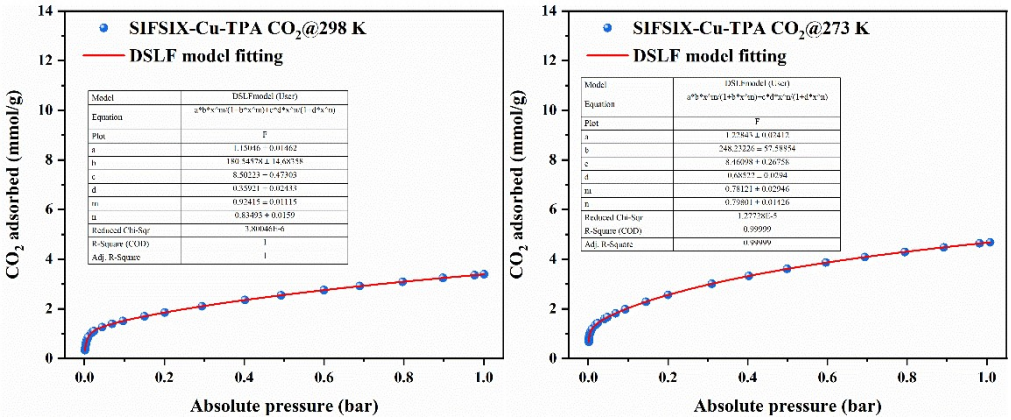

Figure S10. Experimental CO_2 adsorption isotherms at 298/273 K and DSLF model fitting curve of SIFSIX-Cu-TPA.

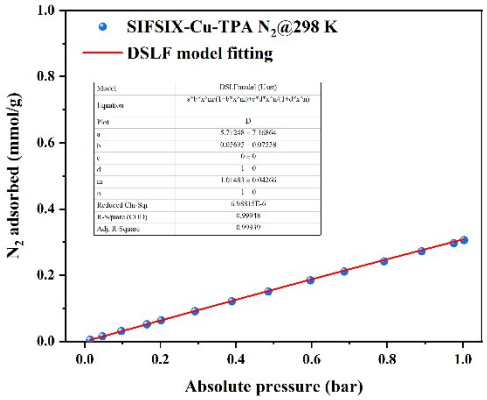

Figure S11. Experimental N_2 adsorption isotherms at 298 K and DSLF model fitting curve of SNFSIX-Cu-TPA.

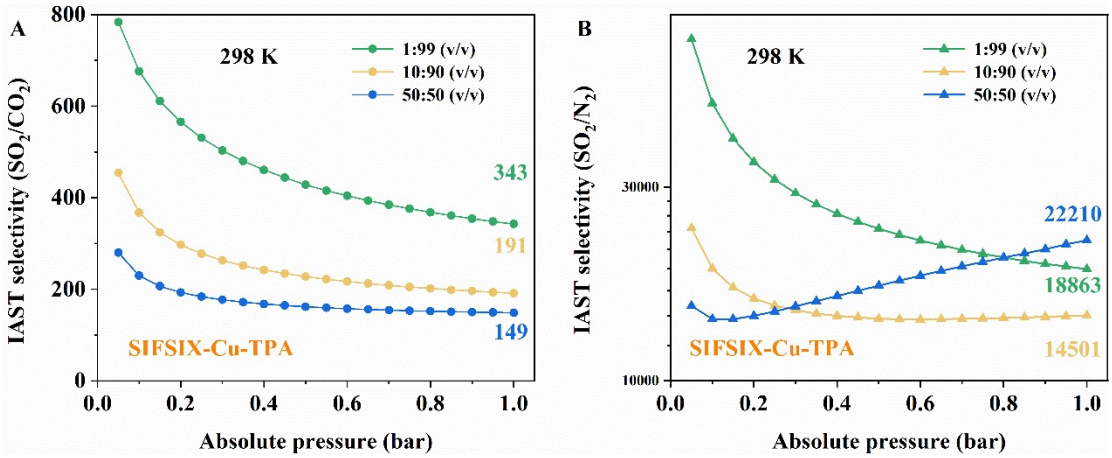

Figure S12. (A) The SO_2/CO_2 and SO_2/N_2 sorption selectivity of SIFSIX-Cu-TPA based on IAST for the 10/90, 1/99 and 50/50 mixture of SO_2/CO_2 or SO_2/N_2 at 298 K.

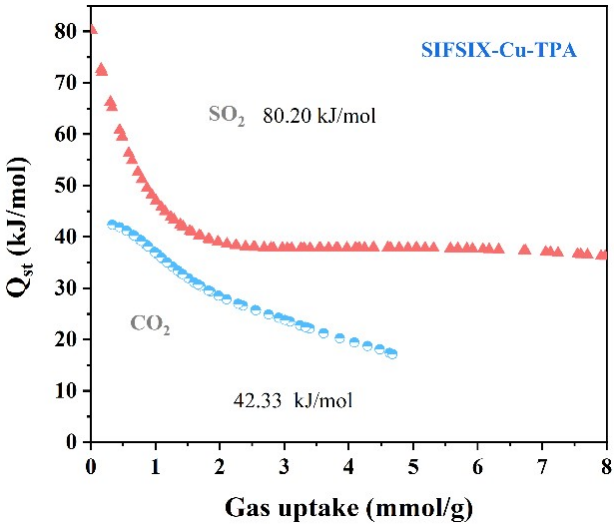

Figure S13. Heat of adsorption (Q_{st}) for both SO_2 and CO_2 as a function of the gas loading amount determined from a viral fit to isotherms collected at 298 K and 273 K.

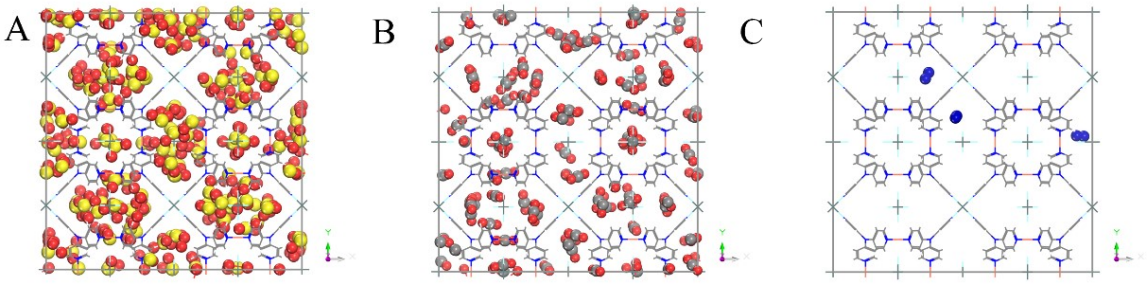

Figure S14. Snapping shots of (A) SO_2, (B) CO_2, and (C) N_2 molecules within the SNFSIX-Cu-TPA structure at 1 bar and 298 K from GCMC simulation results.

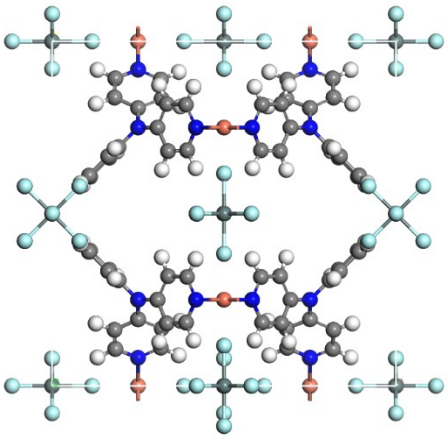

Figure S15. The optimized structure of SNFSIX-Cu-TPA for DFT calculation.

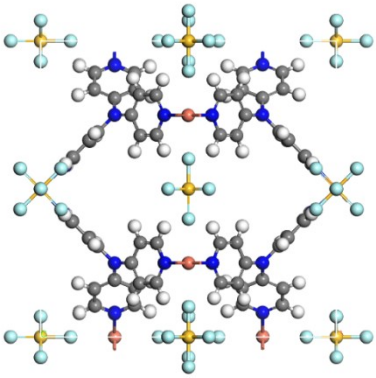

Figure S16. The optimized structure of SIFSIX-Cu-TPA for DFT calculation.

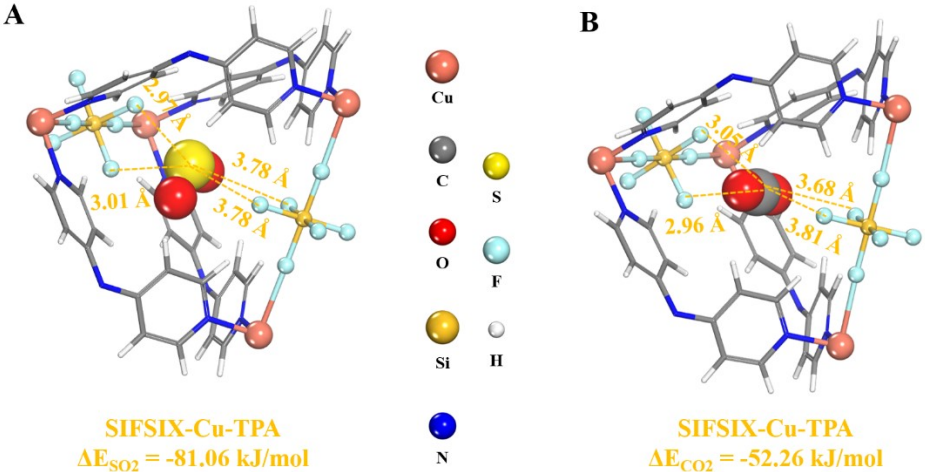

Figure 17. The DFT optimized gas adsorption configuration in SIFSIX-Cu-TPA at Binding sites 1 of SO_2 and CO_2.

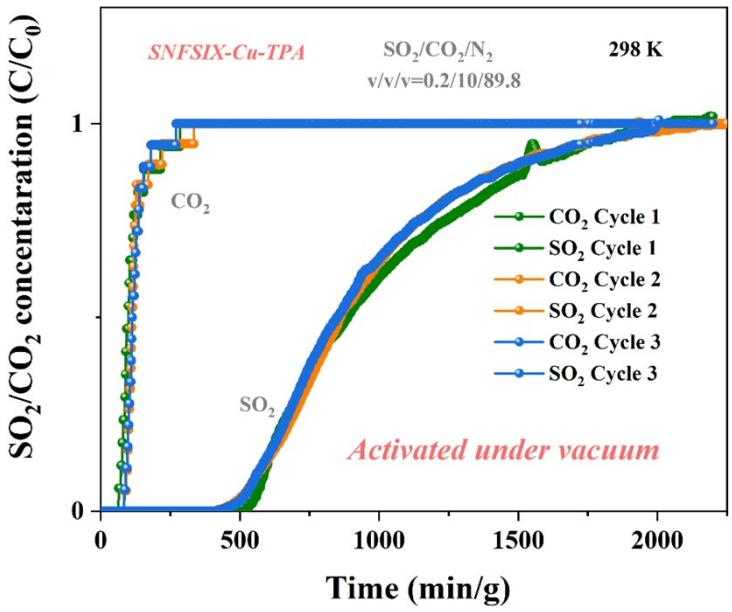

Figure S18. Experimental fix-bed breakthrough curves of three cycling tests in the $SO_2/CO_2/N_2$ mixture on SNFSIX-Cu-TPA at 298 K by activation at room temperature under vacuum for 12 h. (2000 ppm SO_2, 10 vol.% CO_2, 89.8 vol.% N_2; flow rate: 20 mL/min).

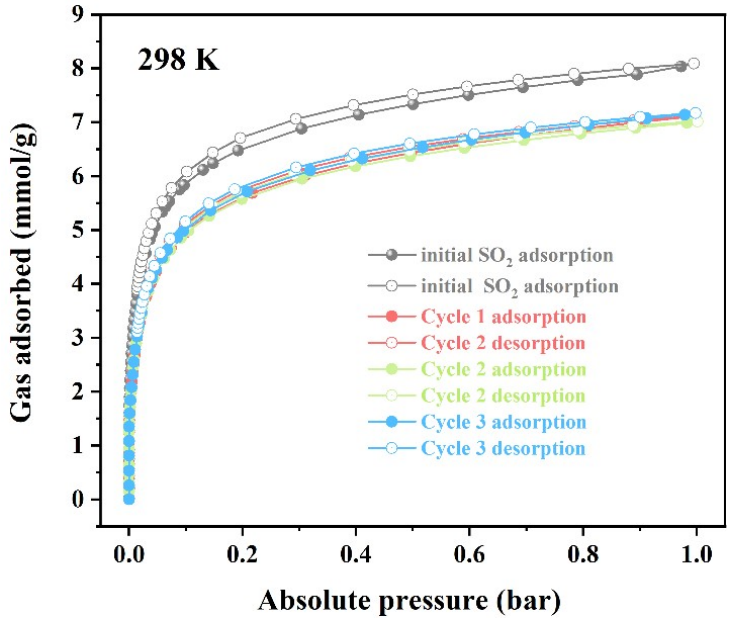

Figure S19. Repeated adsorption-desorption isotherms of SO_2 at 298 K and 1 bar on SNFSIX-Cu-TPA.

Table S1-1. Single crystal data and structure refinement for SNFSIX-Cu-TPA

Compound	SNFSIX-Cu-TPA
Empirical formula	$C_{60}H_{48}Cu_3F_{18}N_{16}Sn_3$
Formula weight	1881.83
Temperature/K	193.00
Crystal system	cubic
Space group	*Pm-3n*
a/Å	17.6072(4)
b/Å	17.6072(4)
c/Å	17.6072(4)
α/°	90
β/°	90
γ/°	90
Volume/Å^3	5458.5(3)
Z	2
ρ calc g/cm^3	1.145
μ/mm^{-1}	7.144
F(000)	1838.0
Crystal size/mm^3	0.13 × 0.12 × 0.1
Radiation	GaKα (λ = 1.34139)
2θ range for data collection/°	6.176 to 120.214
Index ranges	-22 ≤ h ≤ 21, -20 ≤ k ≤ 22, -19 ≤ l ≤ 22
Reflections collected	45287
Independent reflections	1139 [Rint = 0.0715, Rsigma = 0.0202]
Data/restraints/parameters	1139/37/68
Goodness-of-fit on F2	1.073
Final *R* indexes [I>=2σ (I)]	R_1 = 0.0299, wR_2 = 0.0854
Final *R* indexes [all data]	R_1 = 0.0356, wR_2 = 0.0902
Largest diff. peak/hole / e Å-3	0.40/-0.49

Table S1-2. Single crystal data and structure refinement for SIFSIX-Cu-TPA

Compound	SIFSIX-Cu-TPA
Empirical formula	$C_{60}H_{48}Cu_3F_{18}N_{16}Si_3$
Formula weight	1610.03
Temperature/K	193.00
Crystal system	cubic
Space group	*Pm-3n*
a/Å	17.5513(2)
b/Å	17.5513(2)
c/Å	17.5513(2)
α/°	90
β/°	90
γ/°	90
Volume/Å^3	5406.64(18)
Z	2
ρ calc g/cm^3	0.989
μ/mm^{-1}	3.734
F(000)	1622.0
Crystal size/mm^3	0.13 × 0.12 × 0.1
Radiation	GaKα (λ = 1.34139)
2θ range for data collection/°	9.804 to 120.658
Index ranges	-22 ≤ h ≤ 21, -20 ≤ k ≤ 22, -22 ≤ l ≤ 16
Reflections collected	49726
Independent reflections	1127 [Rint = 0.0492, Rsigma = 0.0128]
Data/restraints/parameters	1127/0/52
Goodness-of-fit on F2	1.098
Final *R* indexes [I>=2σ (I)]	R_1 = 0.0533, wR_2 = 0.1642
Final *R* indexes [all data]	R_1 = 0.0589, wR_2 = 0.1726
Largest diff. peak/hole / e Å-3	0.89/-0.31

199

200 **Table S2. The adsorption capacities of SO_2 on various MOFs at 298 K**

Materials	Surface area (m^2/g)	SO_2 uptake at (mmol/g)			Selectivity at 10/90		SO_2 Q_{st} (kJ/mol)	Cycling Stability	Water stability	Ref
		0.002 bar	0.01 bar	1 bar	SO_2/N_2	SO_2/CO_2				
SNFSIX-Cu-TPA	**1169**	**2.22**	**3.33**	**8.09**	**>10000**	**88**	**58.81**	**√**	**√**	**This work**
SIFSIX-Cu-TPA	1243	2.52	3.80	9.15	>10000	191	80.2	-	-	
KAUST-7	280	0.59*	2.04*	2.64*	n/a	n/a	64.8*	√	√	4
KAUST-8	258	0.44*	1.59*	2.91*	n/a	n/a	73.9*	√	√	
SIFSIX-1-Cu	1337	1.80	3.43	11.01	1241	70.7	36.1	√	×	5
SIFSIX-2-Cu-i	735	2.31	4.16	6.90	1017	87.1	38.1	√	×	
SIFSIX-3-Zn	250	0.98	1.68	2.10	371	n/a	45.2	n/a	×	
SIFSIX-3-Ni	368	1.39	2.43	2.74	276	n/a	43.2	n/a	×	
MFM-300-In	1071	1.06	2.17	8.28	2700	50	39.6	√	√	6
MFM-300-Al	1037		-	7.1	n/a	n/a		√	n/a	
MFM-300-Sc	1390		-	9.4	31	31	36.2	√	n/a	
MOF-177	4100	n/a	0.13	25.8	n/a	n/a	n/a	×	×	7
MIL-160	1170	1.93	3.10	7.2	6426		48.68	√	√	
MFM-202a	2220		-	10.2	n/a	n/a	35	×	n/a	8
Co-Gallate	494	2.67	3.37	4.49	55	25	54.1	√	√	9
Mg-Gallate	576	3.99	4.26	5.38	>10000	143	55.6	√	√	
Ni-Gallate	455	4.65	4.87	5.81	>10000	321	60.3	√	n/a	

DUT-67-HCl	1178	<0.5	<1	9.3	9982	33	36.0	√	√	[10]
NU-200	1260		2.52*	11.7			38	√	√	[11]
CC3	402	n/a	n/a	2.78	n/a	n/a	38.5	×	n/a	
RCC3	-	n/a	n/a	12.34	n/a	n/a	82.8	×	n/a	[12]
6FT-RCC3	396	n/a	3.57	13.78	n/a	n/a	43.0	√	n/a	
MFM-190(F)	2538	n/a	n/a	18.3	5.2	n/a	45*	√	n/a	
MFM-101	2300	n/a	n/a	18.7	2.5	n/a	37*	√	n/a	[13]
Viologen-POF	9.4	1.45	4.53	11.3	467	n/a	38.3	√	√	[14]
P(Ph-4MVIm-Br)	158	1.55	2.43	8.12	>10000	>10000	76(cal)	√	n/a	[15]

201

202

203

Table S3. BET report for MFSIX-Cu-TPA

Compound	SNFSIX-Cu-TPA
BET surface area:	1,169.39 ± 1.34 m^2/g
Slope:	0.003720 ± 0.000004 g/cm^3 STP
Y-intercept:	0.000003 ± 0.000000 g/cm^3 STP
C:	1,462.86
Qm:	268.67 cm^3/g STP
Correlation coefficient:	0.9999980
Molecular cross-sectional area:	0.16 nm^2

204

Compound	SIFSIX-Cu-TPA
BET surface area:	1,243.31 ± 4.02 m^2/g
Slope:	0.003500 ± 0.000011 g/cm^3 STP
Y-intercept:	0.000001 ± 0.000000 g/cm^3 STP
C:	6,403.00
Qm:	285.65 cm^3/g STP
Correlation coefficient:	0.9999843
Molecular cross-sectional area:	0.16 nm^2

205

206

Table S4 Comparison of utilization efficiency per anions in anion pillared MOFs used in SO_2 and CO_2 adsorption at 298 K

Materials	MW (g/mol)	Formular	SO_2/MF_6^{2-}(mol/mol)		CO_2/MF_6^{2-}(mol/mol)		Ref
			0.002 bar	1 bar	0.1 bar	1 bar	
SNFSIX-Cu-TPA	**627.28**	**$Cu(SnF_6)(C_{10}H_8N_2)_2$**	**1.39**	**5.07**	**1.01**	**2.30**	**This work**
SIFSIX-Cu-TPA	536.68	$Cu(SiF_6)(C_{10}H_8N_2)_2$	1.35	4.91	0.82	1.82	
KAUST-7	422.91	$Ni(NbOF_5)(C_4H_4N_2)_2$	0.25*	1.12*	0.93*	0.98*	4
KAUST-8	341.09	$Ni(AlOF_5)(C_4H_4N_2)_2$	0.15*	0.99*	0.77*	0.90*	
SIFSIX-1-Cu	517.78	$Cu(SiF_6)(C_{10}H_8N_2)_2$	0.93	5.70	0.21	2.54	
SIFSIX-2-Cu-i	565.78	$Cu(SiF_6)(C_{12}H_8N_2)_2$	1.31	3.90	0.86	2.77	16
SIFSIX-3-Zn	367.64	$Zn(SiF_6)(C_4H_4N_2)_2$	0.36	0.77	0.97	0.90	
SIFSIX-3-Ni	360.96	$Ni(SiF_6)(C_4H_4N_2)_2$	0.50	0.99	1.04	0.96	

207

Table S5 Fitting parameters of DSLF model in SNFSIX-Cu-TPA for adsorption isotherms at 298/273 K

Temp.	Gas	q_1 (mmol/g)	k_1[a]	m	q_2 (mmol/g)	k_2[a]	n	R^2
273 K	SO_2	0.48196	1.97859	5.42854	10.53068	5.25239	0.39068	0.99858
	CO_2	1.27214	884.17124	0.98297	10.15852	0.62293	0.84807	0.99999
	N_2	8.41287	0.05124	0.99471	0	1	1	0.99998
298 K	SO_2	1.42401	14.89018	1.12941	9.07148	2.62589	0.32955	0.99608
	CO_2	1.22931	217.56699	0.98534	11.04964	0.28444	0.8395	0.99999
	N_2	6.18202	0.03961	0.94285	0	1	1	0.99898

208

Table S6 Fitting parameters of DSLF model in SIFSIX-Cu-TPA for adsorption isotherms at 298/273 K

Temp.	Gas	q_1 (mmol/g)	k_1[a]	m	q_2 (mmol/g)	k_2[a]	n	R^2
273 K	SO_2	1.68473	0.60412	3.36577	13.05505	3.57745	0.35413	0.99865
	CO_2	1.22843	248.23226	0.78121	8.46098	0.68522	0.79801	0.99999
298 K	SO_2	3.19408	2.40069	0.78172	9.4933	2.53785	0.3044	0.99694
	CO_2	1.15046	180.54578	0.92415	8.50223	0.35921	0.83493	1
	N_2	5.71248	0.05695	1.10483	0	1	1	0.99948

Table S7 Virial fittings for calculating isosteric heat of adsorption of SO_2 and CO_2 on two MFSIX-Cu-TPA.

Parameters	SNFSIX-Cu-TPA		SIFSIX-Cu-TPA	
	SO_2	CO_2	SO_2	CO_2
a_0	-7101.82764	-4963.12	-8242.777	-4942.85
a_1	2183.17286	444.9077	4741.30174	-1367.63
a_2	-755.93045	-328.01	-2500.06991	3343.615
a_3	107.92025	1238.455	711.11458	-1873.48
a_4	0.03798	-923.341	-117.09322	419.0928
a_5	-1.78157	293.5516	11.05846	-12.8802
a_6	0.19467	-43.3406	-0.55312	-8.36515
a_7	-0.00681	2.44423	0.01131	0.89173
b_0	8.41023	11.05115	5.54337	12.04616
b_1	0.47244	-1.02203	0.92572	-1.28136
R^2	0.99983	0.99933	0.99892	0.99961

Table S8 Calculated the static binding energies in MFSIX-Cu-TPA

Materials	Configuration		E (Hartree)	ΔE (kJ/mol)
SNFSIX-Cu-TPA			-2241.541985	
SIFSIX-Cu-TPA			-2245.226329	
		SO_2	-42.29094325	
		CO_2	-37.76093178	
		H_2O	-17.21979577	
		N_2	-19.89512329	
SNFSIX-Cu-TPA	Site 1	MOF1-SO_2	-2283.861386	-74.7
		MOF1-CO_2	-2279.320947	-47.3
		MOF1-N_2	-2261.447985	-28.6
	Site 2	MOF2-SO_2	-2283.852558	-51.5
		MOF2-CO_2	-2279.316969	-36.9
		MOF2-N_2	-2261.444089	-18.3
SIFSIX-Cu-TPA	Site 1	MOF1-SO_2	-2287.548145	-81.1
		MOF1-CO_2	-2283.007165	-52.3

213

214

References

1 D. Dubbeldam, S. Calero, D. E. Ellis and R. Q. Snurr, *Molecular Simulation*, 2016, **42**, 81–101.

2 J. J. Potoff and J. I. Siepmann, *AIChE Journal*, 2001, **47**, 1676–1682.

3 M. H. Ketko, G. Kamath and J. J. Potoff, *J. Phys. Chem. B*, 2011, **115**, 4949–4954.

4 M. R. Tchalala, P. M. Bhatt, K. N. Chappanda, S. R. Tavares, K. Adil, Y. Belmabkhout, A. Shkurenko, A. Cadiau, N. Heymans, G. De Weireld, G. Maurin, K. N. Salama and M. Eddaoudi, *Nat Commun*, 2019, **10**, 1328.

5 Y. Zhang, P. Zhang, W. Yu, J. Zhang, J. Huang, J. Wang, M. Xu, Q. Deng, Z. Zeng and S. Deng, *ACS Appl. Mater. Interfaces*, 2019, **11**, 10680–10688.

6 K. Tan, P. Canepa, Q. Gong, J. Liu, D. H. Johnson, A. Dyevoich, P. K. Thallapally, T. Thonhauser, J. Li and Y. J. Chabal, *Chem. Mater.*, 2013, **25**, 4653–4662.

7 S. Yang, J. Sun, A. J. Ramirez-Cuesta, S. K. Callear, W. I. F. David, D. P. Anderson, R. Newby, A. J. Blake, J. E. Parker, C. C. Tang and M. Schröder, *Nature Chem*, 2012, **4**, 887–894.

8 M. Savage, Y. Cheng, T. L. Easun, J. E. Eyley, S. P. Argent, M. R. Warren, W. Lewis, C. Murray, C. C. Tang, M. D. Frogley, G. Cinque, J. Sun, S. Rudić, R. T. Murden, M. J. Benham, A. N. Fitch, A. J. Blake, A. J. Ramirez-Cuesta, S. Yang and M. Schröder, *Advanced Materials*, 2016, **28**, 8705–8711.

9 J. A. Zárate, E. Sánchez-González, D. R. Williams, E. González-Zamora, V. Martis, A. Martínez, J. Balmaseda, G. Maurin and I. A. Ibarra, *J. Mater. Chem. A*, 2019, **7**, 15580–15584.

10 X.-H. Xiong, Z.-W. Wei, W. Wang, L.-L. Meng and C.-Y. Su, *J. Am. Chem. Soc.*, 2023, **145**, 14354–14364.

11 W. Gong, Y. Xie, T. D. Pham, S. Shetty, F. A. Son, K. B. Idrees, Z. Chen, H. Xie, Y. Liu, R. Q. Snurr, B. Chen, B. Alameddine, Y. Cui and O. K. Farha, *J. Am. Chem. Soc.*, 2022, **144**, 3737–3745.

12 N. K. Gupta, A. López-Olvera, E. González-Zamora, E. Martínez-Ahumada and I. A. Ibarra, *ChemPlusChem*, 2022, **87**, e202200006.

13 W. Li, J. Li, T. D. Duong, S. A. Sapchenko, X. Han, J. D. Humby, G. F. S. Whitehead, I. J. Victórica-Yrezábal, I. da Silva, P. Manuel, M. D. Frogley, G. Cinque, M. Schröder and S. Yang, *J. Am. Chem. Soc.*, 2022, **144**, 13196–13204.

14 Trace SO2 Gas Capture in Stable 3D Viologen Ionic Porous Organic Framework Microsphere | ACS Applied Materials & Interfaces, https://pubs.acs.org/doi/10.1021/acsami.3c05288, (accessed August 4, 2023).

15 X. Suo, Y. Yu, S. Qian, L. Zhou, X. Cui and H. Xing, *Angewandte Chemie International Edition*, 2021, **60**, 6986–6991.

16 X. Cui, Q. Yang, L. Yang, R. Krishna, Z. Zhang, Z. Bao, H. Wu, Q. Ren, W. Zhou, B. Chen and H. Xing, *Advanced Materials*, 2017, **29**, 1606929.